Polymer Testing 154 (2026) 109085

Contents lists available at ScienceDirect

Polymer Testing

journal homepage: www.elsevier.com/locate/polytest

Tuning the crystallization and polymorphic composition of polypropylene by organo-silane-modified silica

David Jaska [a], Jana Navratilova [a,*], Roman Svoboda [b], Sona Zenzingerova [a], Lenka Gajzlerova [a], Martina Polaskova [a], Roman Cermak [a]

[a] Department of Polymer Engineering, Faculty of Technology, Tomas Bata University in Zlín, Vavreckova 5669, 760 01, Zlin, Czech Republic
[b] Department of Physical Chemistry, Faculty of Chemical Technology, University of Pardubice, Studentská 573, 532 10, Pardubice, Czech Republic

ARTICLE INFO

Keywords:
Polypropylene (iPP)
Silica
Nucleating agent
Organophilization
Organosilanes
Crystallization

ABSTRACT

This work investigates the influence of the alkyl chain length in organosilane-modified silica particles on the crystallization behavior and polymorphic composition of isotactic polypropylene (iPP). Using differential scanning calorimetry (DSC) and wide-angle X-ray scattering (WAXS), blends of iPP with both modified and unmodified SiO_2 particles were analyzed. The kinetics of isothermal crystallization was calculated as well. The results show that organosilane-modified silica promotes the formation of the β-phase, with its proportion increasing alongside the length of the alkyl chain. Besides, the polymorphic composition of iPP is significantly affected by cooling rate and crystallization temperature, with rapid cooling favoring β-phase formation. The highest β-phase content in iPP is achieved using silica modified with octadecyltriethoxysilane (C18) combined with rapid cooling or isothermal crystallization below 134 °C. Notably, these significant effects were achieved at a very low silica concentration of just 0.2 wt percent in the polymer matrix. The combination of Hoffman-Lauritzen theory and Avrami kinetics model was applied to study the influence of silica modification on crystallization kinetics: The effect on morphology proved to be greater than on the crystallization kinetics. This study provides insights into tailoring the crystallization and polymorphism of iPP via surface modification of filler particles in combination with setting of processing conditions.

1. Introduction

Polypropylene is the second most widely used polymer after polyethylene [1,2]. The isotactic form of polypropylene (iPP) finds wide application in many industrial sectors. iPP is a semicrystalline and polymorphic polymer, i.e. it can crystallize into the monoclinic α-phase, trigonal β-phase, and orthorhombic γ-phase [3–5]. During cooling, iPP naturally crystallizes into the most stable α-phase (Tm ≈ 170 °C) [6]. The β-phase offers different mechanical properties without undergoing chemical changes in composition. Primarily, the β-phase exhibits higher toughness and drawability [7–9]. However, the melting point is approximately 15 °C lower than the α-phase [6,10]. Specific β nucleating agents are often utilized to induce crystallization into the β-phase. Typical representatives of β nucleating agents are dicarboxylic acid salts: calcium salt of pimelic or suberic acid (Ca pimelate, Ca suberate), aryl dicarboxamides: N,N-dicyclohexyl-2,6-naphthalenedicarboxamide (commercially NJ Star NU-100) or organic dyes such as β-quinacridone [3,9,11–14].

However, nucleating agents are not the only factors influencing crystallization. Any other additives added to the polymer or impurities present in the polymer can also affect crystallization. These substances cause a reduction in the nucleation energy barrier required to create a nucleation seed [15]. A significant category of such additives is fillers, which are incorporated into polymers to modify their mechanical properties and for economic benefits, as fillers are often substantially cheaper than polymers [16–18]. The determining parameter governing the nucleating capabilities of fillers is the interfacial energy, which refers to the free energy at the interface between the filler and the polymer. This depends on various parameters such as the specific surface chemistry of particles, topology, and morphology of the fillers [19,20].

Isotactic polypropylene is a material with a non-polar nature, meaning it has no affinity with polar substances. This property also affects its interaction with polar fillers. One of the main factors influencing the behavior of inorganic particles in a polymer matrix is their

* Corresponding author. Department of Polymer Engineering, Faculty of Technology, Tomas Bata University in Zlin, Vavreckova 5669, 760 01, Zlin, Czech Republic.
E-mail addresses: jaska@utb.cz (D. Jaska), j1navratilova@utb.cz (J. Navratilova).

https://doi.org/10.1016/j.polymertesting.2026.109085
Received 12 November 2025; Received in revised form 17 December 2025; Accepted 3 January 2026
Available online 3 January 2026

dispersion. Proper dispersion of particles in the matrix is crucial for achieving homogeneous properties and minimizing agglomeration [21–24]. There are two approaches to address this issue. The first option is to modify the polymer matrix by grafting with polar groups (mostly maleic anhydride). These polar groups can interact with polar fillers, thus enhancing their mutual adhesion. Maleic anhydride can also react with surface groups of the filler and create bonds between iPP and the filler, leading to improved dispersion and mutual adhesion [25,26]. The second and more widespread method is surface modification of fillers, known as organophilization. Organophilization, using either bonding or non-bonding agents, is a surface modification process aimed at increasing its affinity or compatibility with organic substances [23,25,26].

Various research teams have focused on studying the influence of both unmodified and organophilized fillers on the crystallization of iPP. It has long been known that talc has very significant nucleating capabilities [27–31] and, in low concentrations, is commonly used for this purpose. On the contrary, calcium carbonate is classified as an inactive filler concerning the crystallization of iPP [28,32–34]. Modifying $CaCO_3$ with stearic acid, however, increase its nucleating activity and can even induce the induce the formation of the β-phase in iPP [35]. Polydimethylsiloxanes, titanates, or fatty acids appear to be less effective modifiers [32,36].

The morphology of iPP filled with silica particles has also been the subject of many studies. It is known that with increasing concentration of silica in iPP, smaller spherulites are formed, and the crystallization temperature shifts towards higher values [21,22]. However, silica particles tend to agglomerate within the iPP matrix, leading to poor miscibility and weak interaction between the filler and the polymer [37]. Therefore, silica is often appropriately modified. A stronger nucleating effect and faster crystallization are observed with modification by octylsilane [38], dimethyldichlorosilane [39and3]-methacryloxypropyltrimethoxysilane [40]. A. K. Schlarb et al. [21] observed that increasing the concentration of silica in polypropylene results in the formation of smaller spherulites and a shift of the crystallization temperature to higher values. Similar trends were also reported by A. Pustak et al. [22], who expanded their study to include more variables. They compared microfillers, both unmodified and modified with organic carbon compounds, with available nanofillers that were either unmodified or modified with methacrylsilane and hexamethyldisilazane. Modified fillers exhibited better dispersion and reduced particle agglomeration compared to unmodified SiO_2. However, an interesting finding was that SiO_2 particles with modified non-polar surfaces induced the formation of larger spherulites than those with polar surfaces, across the entire concentration range. However, in none of the mentioned works, a change in the polymorphic composition of iPP was detected.

This work aims to find out how different lengths of alkyl chains affect the behavior of organosilane-modified silica particles in iPP. The prepared materials are studied both in terms of polymorphic composition and, particularly, in terms of crystallization behavior.

2. Materials and methods

2.1. Materials

The high-isotacticity (>98.5 %) iPP homopolymer Borclean™ HC300BF (MFR 3.3 g/10 min) without containing slip, anti-block, or antistatic additives was supplied by Borealis AG company [41]. Tetraethoxysilane (TEOS), ethanol, ammonium hydroxide NH_4OH, and acetic acid CH_3COOH were used to synthesize SiO_2. For particle modification, four types of alkoxysilanes differing in the length of alkyl chain: methyltriethoxysilane, propyltriethoxysilane, octyltriethoxysilane, and octadecyltriethoxysilane were supplied by Gelest, Inc.

2.2. Sample preparation

The SiO_2 particles were synthesized via the Stöber process [43,44] and then modified with alkoxysilanes [45]. Schematic representation of organosilanol structure attached to a silica surface is shown in Fig. 1. Particle size and size distribution were determined using a Mastersizer 3000+ instrument. The 16 mg of SiO_2 was dispersed in 3 mL demineralized water To improve dispersion, the sample was sonicated for 30 s. The median particle size (D50) is 0.55 μm, D95 is 0.92 μm. The presence of organophilic content was confirmed by thermogravimetric analysis (TGA) [46–48] (see Fig. S1).

Mixtures of iPP with low content of 0.2 wt% (commonly used concentration of nucleating agents [49–51]) of modified or unmodified SiO_2 (Table 1) were prepared by melt mixing at 190 °C using a Haake minextruder with a screw speed of 60 rpm for 5 min. The mixtures were pressed into 1 mm thick plates at 190 °C and then rapidly cooled. These plates were then used for all the analysis.

2.3. X-ray diffraction

The polymorphic composition of the polymer mixtures was studied by wide-angle X-ray scattering (WAXS) on an XRDynamic 500 instrument, Anton Paar. The measurement was performed in reflection mode using CuKα (λ = 0.154 nm) radiation in the angular range 2θ from 5 to 30°.

The total crystallinity was calculated by integrating the area of crystalline peaks and their ratio to the sum of crystalline and amorphous regions. Crystallinity was determined using the relation:

$$Xc = \frac{\sum A_C}{\sum A_C + \sum A_A} \tag{1}$$

where A_C is the integrated area of the crystalline reflections and A_A is the area of the diffuse amorphous component. The relative content of the β-phase was evaluated based on the ratio of the intensity of the principal β(300) diffraction peak at $2\theta \approx 16.1°$ to the sum of the intensities of the characteristic α(110), α(040), α(130), and β(300) peaks:

$$K_\beta = \frac{A^\beta_{300}}{A^\beta_{300} + A^\alpha_{110} + A^\alpha_{040} + A^\alpha_{130}} \tag{2}$$

where A^β_{300} is the intensity of the β-phase, and $A^\alpha_{110}, A^\alpha_{040}, A^\alpha_{130}$ are the respective intensities of the main α-phase peaks. The calculation is performed after background subtraction and deconvolution of the diffraction profiles [52–54].

2.4. Differential scanning calorimetry

The isothermal and non-isothermal crystallization was studied on a Mettler Toledo DSC 1 instrument with an automatic sample feeder and under N_2 atmosphere (20 ml/min).

To measure non-isothermal crystallization, the samples punched into circular specimens with a diameter of 6 mm and a mass of approximately 5 mg were first heated from 30 °C to 210 °C. After 5 min at 210 °C, cooling to 30 °C was performed at various cooling rates (2, 5, 10, 20, and 40 °C/min). To study isothermal crystallization, the samples were heated from 30 °C to 210 °C. After 5 min at 210 °C the samples were cooled to the crystallization temperature at a rate of 60 °C/min, at which the sample was maintained throughout the crystallization period. All heating regimes were performed at a heating rate of 10 °C/min.

The crystallinity from DSC measurement was calculated by measuring the enthalpy of melting ΔH_m obtained from the area under the melting peak, and comparing it to the reference value for 100 % crystalline polypropylene ΔH^*_m:

$$X_C = \frac{\Delta H_m}{\Delta H^*_m} \tag{3}$$

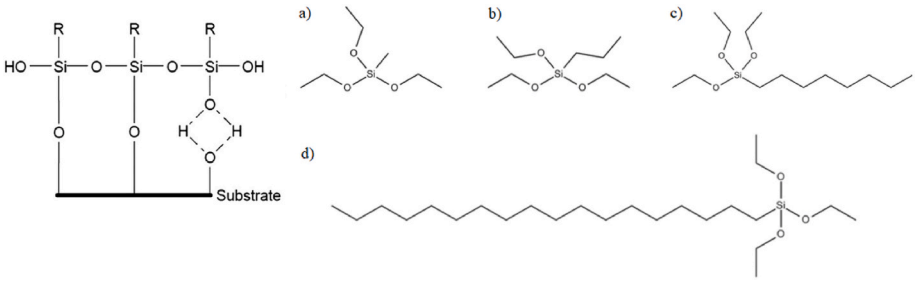

Fig. 1. Organosilanol structure attached to a silica surface [42] where R is -CH_3 in methyltriethoxysilane (a), -C_3H_7 in propyltriethoxysilane (b), -C_8H_{17} in octyltriethoxysilane (c), and -$C_{18}H_{38}$ in octadecyltriethoxysilane (d).

Table 1
Nomenclature of polymer mixtures.

Samples	Modifier	Modifier designation
PP	–	–
PP-SiO_2	Unmodified	–
PP-SiO_2-C1	Methyltriethoxysilane	C1
PP-SiO_2-C3	Propyltriethoxysilane	C3
PP-SiO_2-C8	Octyltriethoxysilane	C8
PP-SiO_2-C18	Octadecyltriethoxysilane	C18

where ΔH_m is the experimental heat of melting (in J/g), and ΔH_m^* is the literature value for a fully crystalline sample, typically taken as 207 J/g[49,50]

To determine the β-phase content, the melting endotherms associated with the β- and α-phases are separated by assigning the individual melting peaks in the DSC curve. The areas under the respective peaks correspond to the enthalpies of melting for the β-phase (ΔH_β) and the α-phase (ΔH_α). The relative proportion of the β-phase is then calculated as:

$$K_\beta = \frac{\Delta H_\beta}{\Delta H_\beta + \Delta H_\alpha} \quad (4)$$

Where ΔH_α and ΔH_α are the areas under the melting peaks for the β- and α-phases, respectively. This approach enables quantification of both the total degree of crystallinity and the fraction of the β-phase in polypropylene samples using DSC analysis [55–57].

3. Results and discussion

3.1. Crystalline morphology

To study the polymorphic composition, measurements were performed by wide-angle X-ray scattering. Fig. 2 presents the X-ray spectra of the studied mixtures. The dominant diffraction maxima correspond to reflections of the α-phase of iPP and the peaks are located approximately at 2θ = 14°, 17°, 18.5° and 21,9°, i.e. typically for the (110), (040), (130) and (131, 041) planes. The peak at 21.1° is not clearly assignable to a single phase – it is the sum of α-phase (111) and β-phase (301). The β peak (300) at 2θ = 16,1° s key for identifying and quantifying the β-phase, so it is shown in detail.

The crystallinity of all materials varies within a narrow range of 58–61 %. The presence of organophilized particles does not affect the overall crystallinity of the polymer unlike the polymorphic composition. A significant content of the β-phase, namely 19 %, is observed in the PP-SiO_2-C3 mixture, and the proportion of the β-phase further increases with the increasing length of the alkyl chain of the used organosilane. The highest content of the β-phase is recorded in the PP-SiO_2-C18 mixture (34 %). There is no observable difference between unmodified particles and particles modified using C1, the organosilane with the shortest alkyl chain. Therefore, it can be seen that the length of the alkyl

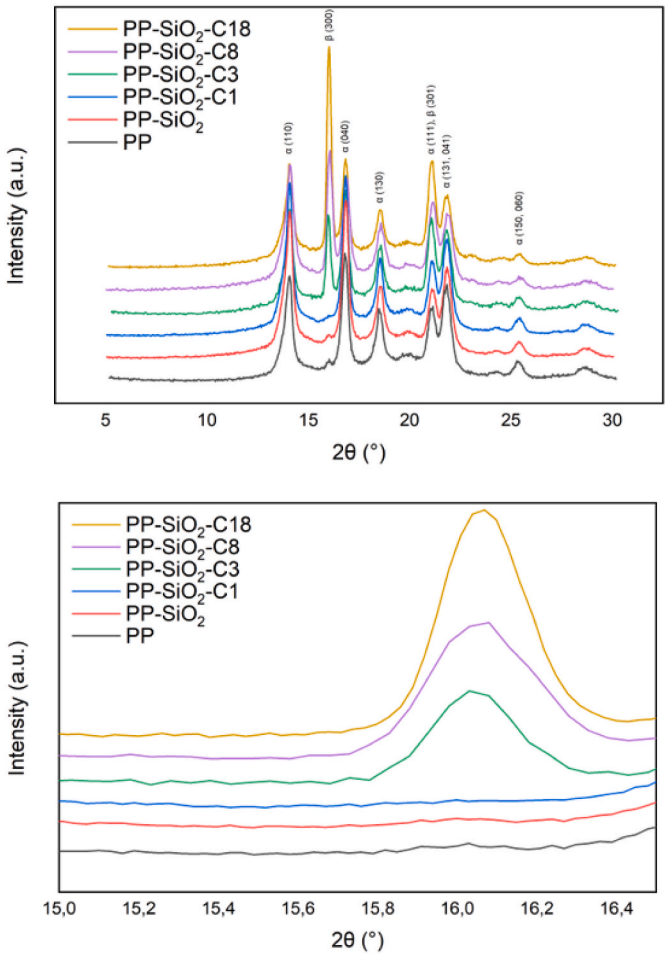

Fig. 2. WAXS spectra of prepared samples (up) and a detailed view of the β peak (down).

chain of the organosilane has an essential influence on the polymorphic composition of PP.

The results of polymorphic composition obtained from WAXS can be compared with the results of the first melting on DSC, i.e., the melting of the material that has not been deprived of its thermal history. Comparing the calculated amount of the β-phase from Table 2 with the first melting profile in Fig. 3, the DSC results confirm that rapidly cooled PP, PP-SiO_2, and PP-SiO_2-C1 samples show almost no β-phase content. The β-phase content is observed by a peak around the temperature of 155 °C in samples where an organosilane with a longer alkyl chain was used. DSC also confirmed that the largest content of the β-phase is present in PP-SiO_2-C18. By subtracting the proportional DSC melting signal of PP from the melting signal of the modified samples, the ratio

Table 2
The proportion of the β-phase of iPP in the studied mixtures.

Samples	Xc (%)	β-phase/WAXS (%)	β-phase/DSC (%)
PP	61	1	–
PP-SiO_2	61	2	–
PP-SiO_2-C1	62	2	–
PP-SiO_2-C3	58	19	22
PP-SiO_2-C8	59	23	16
PP-SiO_2-C18	59	34	33

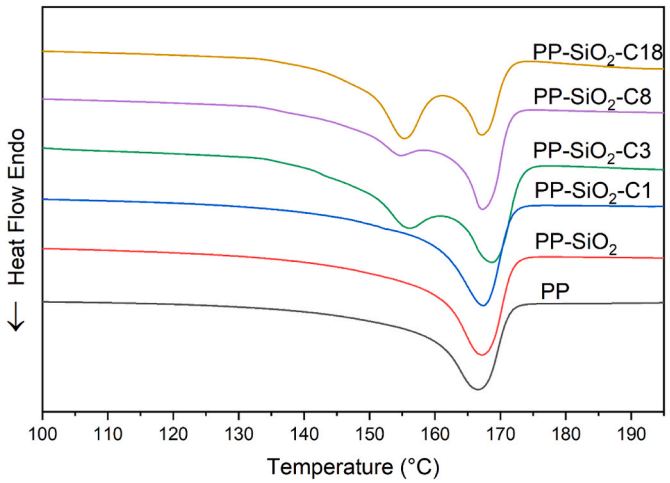

Fig. 3. DSC crystallization endotherms of prepared samples – first melting.

between the melting enthalpies of the two crystalline phases was obtained. Assuming that both pure polymorphic phases (α and β) exhibit similar ΔH_m^{eq}, the content of the β-phase can be estimated based on this calculation – the results are listed in Table 2 (the estimated errors of the β-phase determination are <5 %). The general agreement between the WAXS and DSC results regarding the content of the β-phase further confirms the crucial influence of the high cooling rate (as a supplemental aspect to the presence of the β-nucleating agents) for the dominant formation of the β-phase in isotactic polypropylene.

3.2. Non-isothermal crystallization and melting

The effect of modified silica on crystallization was first studied under non-isothermal conditions. Cooling thermograms of two representatives of PP-SiO_2 and PP-SiO_2-C18 are shown in Fig. 4. The results of the other mixtures are not shown, as the course of crystallization is very similar in all cases, as seen in and Fig. 5 and Table S1. As the cooling rate increases, the crystallization temperature Tc naturally decreases. A similar trend is observed in all cases, i.e., the crystallization temperatures at each cooling rate are very similar for all samples. The presence of unmodified

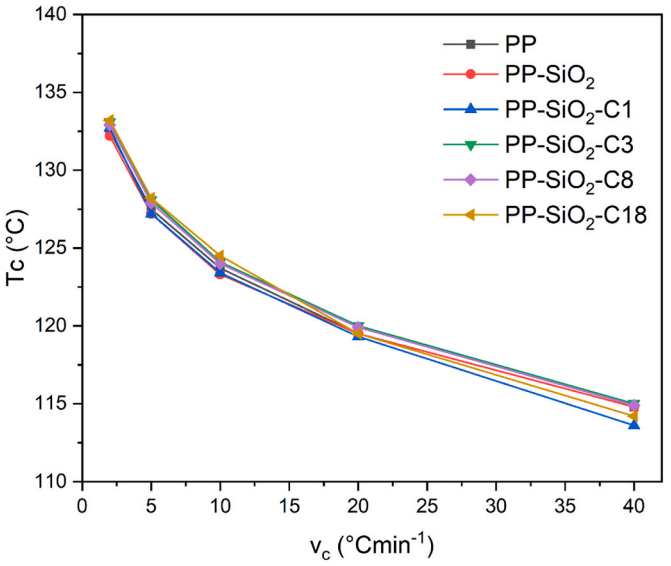

Fig. 5. Dependence of the crystallization temperature Tc on the rate of cooling rate v_c.

or modified silica particles has a negligible effect on the development of the Tc under given conditions. More interestingly, it is to observe the melting behavior and thus supermolecular composition of mixtures crystallized from the melt at different cooling rates. These heating scans are shown in Fig. 6.

Here, a dominant endothermic peak can be observed, corresponding to the melting of polypropylene in the α-modification, located approximately in the range of 165–170 °C. With increasing cooling rate, a second peak appears around 150–155 °C, which can be attributed to the melting of the β-phase of polypropylene. The melting curves after non-isothermal crystallization at low cooling rates of 2 °C/min and 5 °C/min show no significant differences independently of silica presence. The cooling rate was slow enough for all melt to crystallize into the α-phase. The first differences between the mixtures are observed at a cooling rate of 10 °C. Upon heating such crystallized mixtures, distinct melting peak of the β-phase can be observed in PP-SiO2-C18. This is even more evident after faster cooling at 20 °C/min, where the melting peak of the β-phase is well observable in all mixtures that use modified silica. A hint of the β-phase presence is also observed in PP-SiO_2. Pure PP shows little to no indication of the β-phase. This changes in the fastest cooled samples, where the β-phase is observable in all cases, including neat PP. It has long been known that a higher content of the β-phase can be achieved even in pure polypropylene when rapidly cooled [58,59]. However, the proportion of the β-phase is greater in mixtures where modified silica was used. The organophilization of SiO_2 thus enhances the effect of rapid cooling on the formation of the β-phase. Determining the specific representation of the β-phase from DSC exotherms is

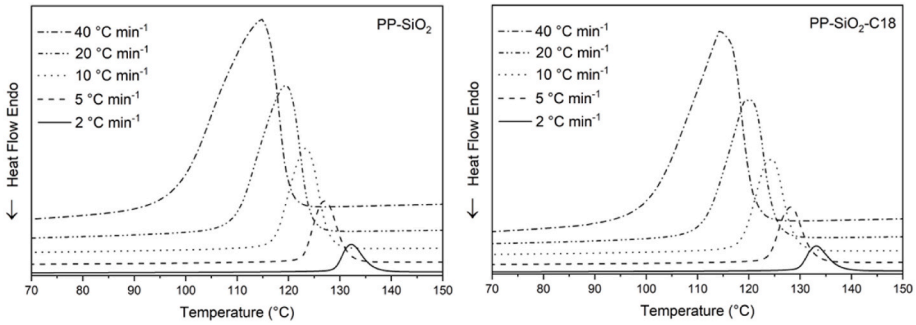

Fig. 4. DSC crystallization exotherms of PP-SiO_2 (left) and PP-SiO_2-C18 (right) samples at different cooling rates.

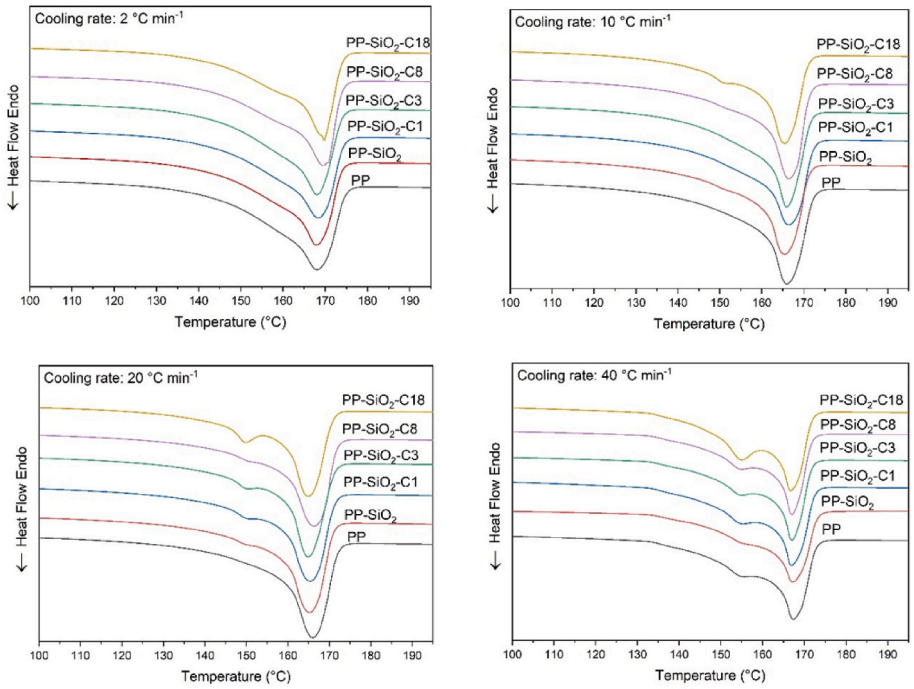

Fig. 6. DSC fusion endotherms under a heating rate of 10 °C/min prepared by non-isothermal crystallization.

practically impossible because during cooling, both phenomena, the crystallization of the α-phase and the crystallization of the β-phase, overlap [60]. It is also difficult to define the exact contents of individual polymorphs from heating curves due to possible recrystallization processes. Nevertheless, the profile of the heating curve gives good insight into qualitative composition of the supermolecular structure. In the case of prepared mixtures, the most distinct β-phase peak is always observed with the organosilane with the longest alkyl chain, C18. Thus, the long alkyl chain allows the creation of a suitable template for the growth of the trigonal β-phase of polypropylene on the surface of silica. More in general, it can be stated that length of the alkyl chain of the used organosilane while modifying the silica influence the morphology of iPP.

3.3. Isothermal crystallization and melting

Isothermal crystallization enables a more detailed study of crystallization kinetics and was performed as a supplement to non-isothermal crystallization. The exotherms of pure PP and mixtures at different crystallization temperatures and corresponding crystallization S-curves created by integrating the heat flow curve are illustrated in Fig. 7, the dependence of crystallization half-time on crystallization temperature is shown in Fig. 8. Corresponding values are listed in Table S2.

The description of the crystallization rate often utilizes the crystallization half-time $t_{0,5}$. This is the time at which 50 % of the polymer is crystallized and is derived from the calculation of relative crystallinity. It is not accurate to evaluate the crystallization half-time from the peak of the crystallization curve, as this peak may not be symmetrical. The crystallization half-time typically lies beyond the peak of the curve [61, 62].

In the case of the isothermal measurements performed at low temperatures (128 and 130 °C), the evolved heat associated with the formation of the crystalline phase largely overlapped with the DSC artifact signal (in this case also exothermic) corresponding to the transition from the non-isothermal to the isothermal conditions. This parasitic signal was filtered out utilizing the standard thermo-kinetic procedure, i.e., via subtraction of the similar but fully separated heat flow profile obtained for the isotherm at 134 °C. Owing to the excellent reproducibility of the

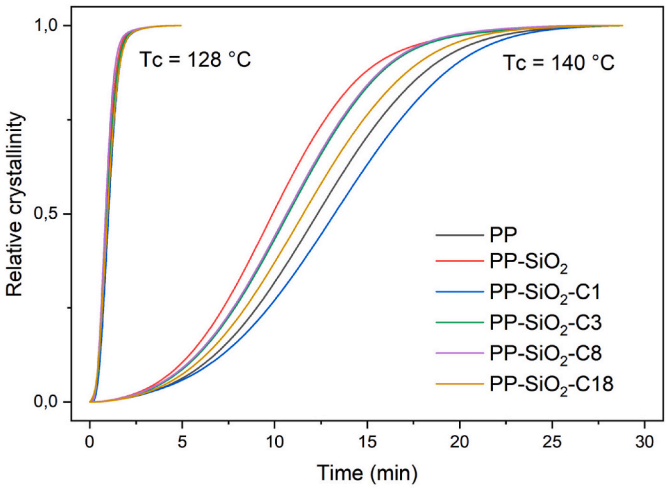

Fig. 7. Relative crystallinity at different crystallization temperatures.

DSC data, which was also confirmed for the onset edge of this parasitic signal, only negligible scatter was obtained in the overlap region – the negative scatter values were cut off, the positive values were left as produced. This way, a reproducible and physically meaningful method was used to subtract the thermokinetic background (baseline) and obtain the pure crystallization signal.

The shortest crystallization half-time $t_{0,5}$ is observed in PP-SiO_2 in most crystallization temperatures (Fig. 8). The presence of silica speeds up the crystallization, but most significantly in the unmodified variant. As for mixtures containing organophilized SiO_2 particles, a decrease of crystallization half-time is also observed with the exception of PP-SiO_2-C1. It is apparent that silica modified by organosilane with the shortest alkyl chain slows down crystallization. This is particularly noticeable at higher crystallization temperatures. At Tc = 140 °C, PP-SiO_2-C1 crystallizes 24 % slower than PP-SiO_2. Similar differences are observed at Tc = 136 and 138 °C. A possible explanation is that the unmodified SiO_2 particles possess a higher number of active sites for rapid nucleation of

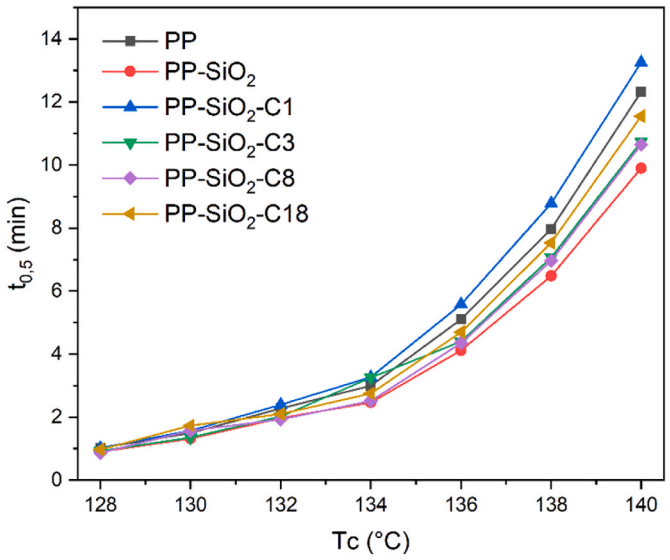

Fig. 8. Dependence of the crystallization half-time on the crystallization temperature.

iPP, while modification with organosilanes (particularly those with short chains) may partially "coat" the particles and thus reduce the number of available nucleation centers. At the same time, longer alkyl chains render the surface more nonpolar, which can limit direct nucleation interactions but improve dispersion and promote the formation of the specific β-phase, which crystallizes under different conditions. The overall effect therefore depends on the balance between nucleation activity, dispersion, and the surface chemistry of the modified particles. In the case of other modified silica particles, the crystallization half-time is shorter but it cannot be definitively inferred that the length of the alkyl chain of the organosilane affects $t_{0,5}$ with specific trend.

After controlled isothermal crystallization, the samples were heated up to observe the melting thermograms, see Fig. 9 and S3. The dominant peak at temperature approx. 166 and 170 °C, depending on crystallization temperature, is observed in all cases. This peak is associated with melting of α-phase and mostly is not symmetric showing the shoulder at lower temperatures. In samples containing organosilanised silica crystallized at lower temperatures, an additional peak at temperature of approx. 154 °C can be identified and points out the presence of β-phase. Thus, the modification of silica by organosilane can increase the nucleation activity into β-phase, however with strong dependence of crystallization temperature; the lower the crystallization temperature, the more significant melting peak of β-phase. The threshold temperature appears at 134 °C, where the β peaks are still visible and can be unambiguously identified. At higher crystallization temperatures, the polymer crystallizes primarily into the α-phase, similar to PP and PP-SiO_2. However, it should be noted, that the asymmetry of the melting peak of the α-phase may also indicate the presence of a small amount of the β-phase, along with the presence of less perfect crystals of the α-phase. The values of melting temperatures (taken as a maximum of melting peaks) are listed in Table 3. As mentioned before, the materials PP and PP-SiO_2 show very similar profile of melting curves, accordingly, the melting temperatures differ only slightly by 0.5 °C. Therefore, simply using heterogeneous SiO_2 particles in the polymer matrix is insufficient to change the polymorphic composition. The β-nucleation effect, according to presented results, is achieved only when these heterogeneous particles are modified using organosilanes and, in addition, suitable crystallization temperature is applied. The need for appropriate setting of crystallization conditions with regard to the β-nucleating agent used is a common phenomenon [63,64]. In general, the effectiveness of nucleating agents can be enhanced by adjusting the crystallization conditions, even in the case of highly effective and commercially used agents [65,66].

Considering the mutual relationship between the isothermal and non-isothermal crystallization processes, it can be inferred from the comparison of the corresponding melting peaks (Figs. 3 and 9) that the formation of the β-phase occurs in a relatively complex manner. Following the fast cooling during the isothermal crystallization experiments, significant amounts of the β-phase start to form at T ≤ 134 °C. On the other hand, during the non-isothermal crystallization experiments, similar amounts of the β-phase form during cooling at 10–20 °C/min, i.e., at temperatures T ≤ 125–128 °C. This discrepancy suggests that the high cooling rate is crucial for the formation of the β-phase. Since the growth rate of the β-phase is known to exceed that of the α-phase only within the $T_{\alpha\beta}$–$T_{\beta\alpha}$ critical window (approx. 105–141 °C) [67], and since the present β-nucleating agents further enhance the nucleation rate of the β-form, the high cooling rate appears to primarily function as a suppression of the (otherwise dominant) nucleation&growth of the α-phase. Despite the crystal growth rate conditions being theoretically favorable for the dominant crystallization of the β-phase within the $T_{\alpha\beta}$–$T_{\beta\alpha}$ critical window, no β-phase forms in the pure PP even during isothermal annealing at 128 °C. This stresses the utmost importance of the nucleation process (as opposed to the consequent growth of the formed nuclei), where only the addition of the nucleating agents increases the rate of the β-nucleation high enough for the process to be competitive with the α-nucleation.

3.4. Crystallization kinetics

A potential influence of the organophilized SiO_2 particles on the crystallization kinetics of iPP was explored for the isothermal crystallization data depicted in Fig. 7 (note that the isothermal data were selected due to the guaranteed absence of potential thermal gradients during the DSC measurement). The crystallization kinetics was described in terms of the standard solid-state kinetic equation for DSC [68]:

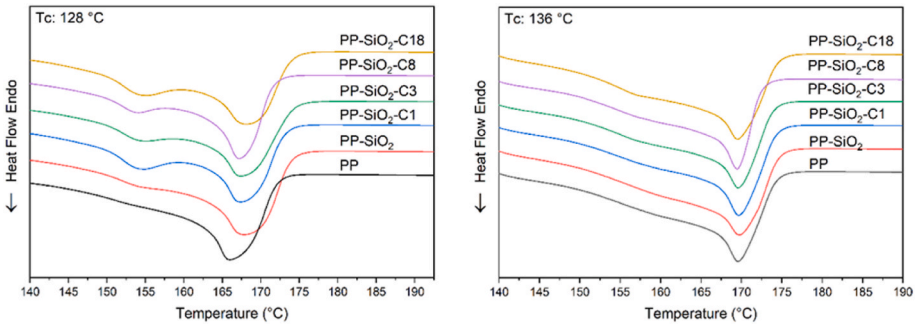

Fig. 9. DSC melting endotherms of the studied mixtures crystallized at 128 °C (left) and 136 °C (right) (for 130, 132, 134, 138 and 140 see Fig. S3).

Table 3
Melting point of the α-phase and β-phase of the studied mixtures.

Tc	PP		PP-SiO_2		PP-SiO_2-C1		PP-SiO_2-C3		PP-SiO_2-C8		PP-SiO_2-C18	
	Tm_α	Tm_β	Tm_α	Tm_β	Tm_α	Tm_β	Tm_α	Tm_β	Tm_α	Tm_β	Tm_α	Tm_β
128	166.3	–	166.8	–	166.5	153.4	166.6	153.4	166.0	153.1	167.6	153.6
130	167.0	–	167.0	–	166.6	154.1	166.9	154.3	166.6	153.8	167.2	154.1
132	167.6	–	167.5	–	167.5	155.1	167.8	155.1	167.4	154.6	167.9	155.1
134	168.5	–	168.6	–	168.6	–	168.6	156.0	168.4	155.6	168.7	155.9
136	169.6	–	169.8	–	169.8	–	169.7	–	169.4	–	169.6	–
138	170.6	–	170.5	–	170.7	–	170.5	–	170.4	–	170.6	–
140	171.4	–	171.5	–	171.6	–	171.5	–	171.4	–	171.6	–

$$\Phi = \Delta H_c \cdot \frac{d\alpha}{dt} = \Delta H_c \cdot K(T) \cdot f(\alpha) \tag{5}$$

where Φ is the heat flow recorded by the DSC instrument, ΔH_c is the crystallization enthalpy, α is the degree of conversion from the amorphous (undercooled liquid) into the crystalline phase, t is time, dα/dt is the rate of conversion, K(T) is the temperature-dependent rate constant, and f(α) is a suitable kinetic model. As is customary for polymeric materials, the rate constant was expressed within the framework of the Hoffman-Lauritzen theory [69]:

$$K(T) = A \cdot exp\left(-\frac{U}{R(T - T_\infty)}\right) exp\left(-\frac{K_G}{T\Delta Tf}\right) \tag{6}$$

where A is a pre-exponential factor, U is the activation energy of the segmental jumps in polymer chains (considered to be 6300 J/mol for the majority of polymeric materials [69]), R is the universal gas constant, T_∞ is the temperature under which all motions associated with viscous flow are supposed to be significantly higher than the given experimental time scale for the crystal growth (customarily $T_\infty = T_g - 30$ °C, where T_g is the glass transition temperature), K_G is the kinetic parameter associated with nucleation, ΔT is the undercooling (defined as $\Delta T = T_m^{eq} - T$, where T_m^{eq} is the equilibrium melting temperature), and f is the correction factor defined as $f = 2T/(T_m^{eq} + T)$. For the present data, the well-known Avrami model [70–73] was utilized:

$$f(\alpha) = m(1-\alpha)[-\ln(1-\alpha)]^{1-\left(\frac{1}{m}\right)} \tag{7}$$

where m is the Avrami kinetic exponent representing the nucleation conditions and crystal growth geometry. Prior to the kinetic calculations based on Equations (5)–(7), the applicability of the Avrami model was verified using the characteristic kinetic function z(α) [74]:

$$z(\alpha) = \Phi \cdot t \tag{8}$$

For the Avrami model to be valid, the maximum of this function $\alpha_{max,z}$ needs to occur at $\alpha \approx 0.632$; the particular limits are 0.620–0.665 for the $r^2 = 0.999$ correlation, and 0.585–0.705 for the $r^2 = 0.995$ correlation. The $\alpha_{max,z}$ values determined for the present materials (averaged over all T_cs) are listed in Table 4; as can be seen, the obtained $\alpha_{max,z}$ values are borderline or just outside the $r^2 = 0.999$ interval, which confirms the applicability of the Avrami model (Eq. (7)).

In the present study, a generalized reduced gradient (GRG) nonlinear optimization method based on the combination of Equations (3)–(7) was used to fit the isothermal crystallization data. To reduce the number of variables, the kinetic parameters K_G and A were extracted from the experimental data in the preliminary step. Assuming a similar degree of conversion being reached at $t_{0.5}$ under all experimental conditions (verified for the present data), the following linearization can be derived from Equation (6):

$$ln(1/t_{0.5}) + \frac{U}{R(T_c - T_\infty)} = lnA - \frac{K_G}{T_{0.5}\Delta Tf} \tag{9}$$

where $T_{0.5}$ is the temperature corresponding to $t_{0.5}$. This evaluation is for the present data shown in Fig. 10. The linear fits of the data gave K_G and

Table 4
Values of $\alpha_{max,z}$, K_G and A determined for the present composites.

Samples	$\alpha_{max,z}$ (−)	K_G	$\ln(A/s^{-1})$
PP	0.670 ± 0.012	66500 ± 3800	4.45 ± 0.33
PP-SiO_2	0.663 ± 0.004	64000 ± 3500	4.41 ± 0.30
PP-SiO_2-C1	0.676 ± 0.017	68100 ± 4400	4.53 ± 0.38
PP-SiO_2-C3	0.673 ± 0.021	65200 ± 4400	4.43 ± 0.39
PP-SiO_2-C8	0.672 ± 0.015	65000 ± 4100	4.45 ± 0.36
PP-SiO_2-C18	0.664 ± 0.012	64400 ± 3900	4.31 ± 0.34

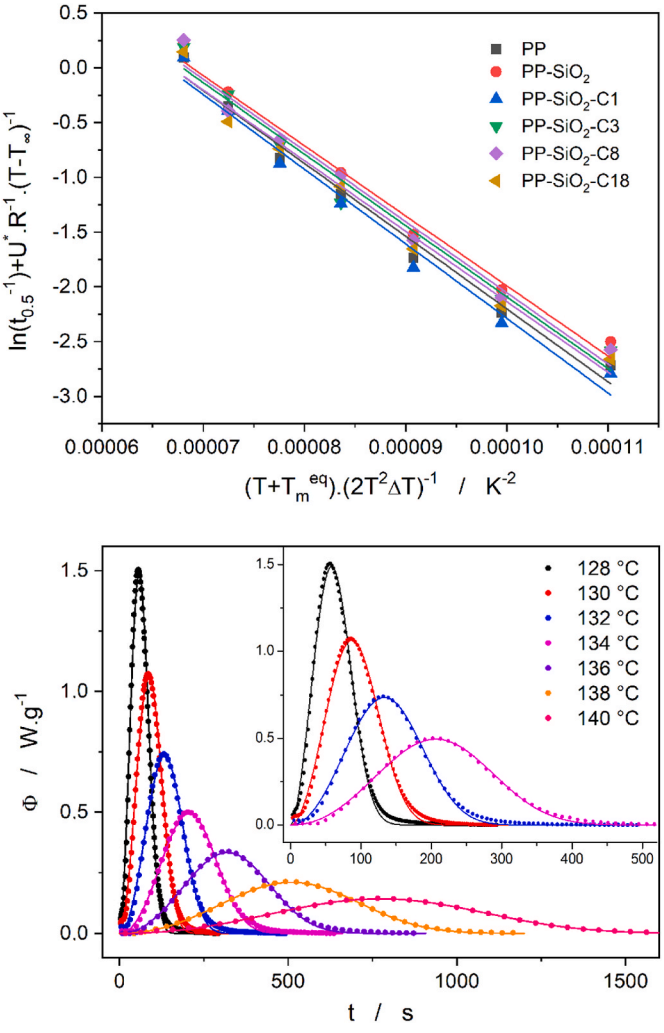

Fig. 10. Evaluation of K_G and A according Eq. 5 (up) and demonstration of the quality of the fit of the isothermal crystallization data (obtained for pure iPP) by the Avrami-Hoffman-Lauritzen model, i.e., the combination of Eqs. (1)–(3) (down).

A values listed in Table 4. Considering the mild curvature of the data depicted in Fig. 10 (which most probably indicates the transition between the II and III nucleation/growth regimes, as defined by the Hoffman theory [69]), an optional solution to the linearization represented by Equation (9) would be the determination of the temperature-dependent K_G and A parameters. However, it can be shown that the parameters K_G and A exhibit high mutual correlation in Equation (6), and thus compensate each other. Hence, K_G was set to be constant (as listed in Table 4), and A was set as a variable during the non-linear optimization. The T_g and T_m^{eq} values were taken from literature on iPP ($T_g \approx 0$ °C [75], $T_m^{eq} \approx 186.2$ °C [76]); considering the high similarity of the crystallization and melting DSC signals obtained for pure iPP and organosilane-modified iPP/silica composites, an assumption of the akin similarity of T_g and T_m^{eq} values was adopted.

Very high quality (correlation coefficients ranging between 0.9980 and 0.9995) of the fits of the experimental data by the combination of Equations (5)–(7) was obtained for all isothermal DSC curves. In Fig. 10, an example of the experimental data being fit by the Avrami-Hoffman-Lauritzen model is shown for the pure iPP material. Qualitatively identical fits were also obtained for the iPP/silica composites. As can be seen, the only minor systematic discrepancy occurs in the endset region of the crystallization peaks, where at low T_cs, the model slightly underestimates the prediction (as shown in the inset of the given figure). The base kinetic parameters (set variable during the optimization) representing the crystallization behavior of the present composites are depicted in Fig. 11. The crystallization enthalpy varies between ~95 and 101 J/g, which (compared to the literature value of the equilibrium melting enthalpy $\Delta H_m^{eq} = 207$ J/g for 100 % crystalline iPP) indicates that the overall crystallinity achieved during the isothermal annealings could be estimated to $X_c \approx 46$–49 %. However, this estimate can be burdened by a relatively large error due to the expected temperature evolutions of ΔH_c and ΔH_m (in accordance with the Kirchhoff's law based on the non-constant temperature dependence of heat capacity). The Avrami exponent was, in all cases, very close to 3, which indicates three-dimensional crystallites growing from heterogeneously formed nuclei. At low T_cs, a slight decrease of the Avrami exponent $m \approx 2.5$–2.8 occurs, which may be associated with the transformation rate starting to be controlled by diffusion instead of the reaction on the interface [77]. Such interpretation may be physically explained by the high transformation rate associated with the high undercooling, where the higher importance of diffusion is related to the far-reaching morphological perturbations during the re-organization into the crystalline phase. The last graph in Fig. 11 depicts the values of the pre-exponential factor A determined for the present composites. The strong temperature dependence is directly related to the compensation effect between K_G and A, as was discussed above. No significant development with the organosiloxane treatment (or the silica addition itself) can be identified.

4. Conclusion

The crystallization behavior and polymorphic composition of iPP and iPP mixtures with modified and unmodified SiO_2 particles have been described. The organophilization of SiO_2 particles influences the resulting polymorphic composition but depends on processing conditions as well. In laboratory-prepared mixtures that were rapidly cooled, the β-phase was detected, and its quantity was the highest when the longest alkyl chain of the used organosilane was applied. Cooling rate significantly affects the polymorphic composition (despite not altering the crystallization kinetics significantly), as confirmed by both isothermal and non-isothermal crystallization results. In the case of isothermal crystallization, the β-phase begins to form at a crystallization temperature lower than 134 °C. For non-isothermal crystallization, the β-phase forms already at a cooling rate of 10 °C/min for the PP-SiO_2-C18 mixture containing silica modified with the organosilane bearing the longest alkyl chain. However, higher cooling rates are needed for other mixtures with modified organosilanes. Organosilane-modified particles

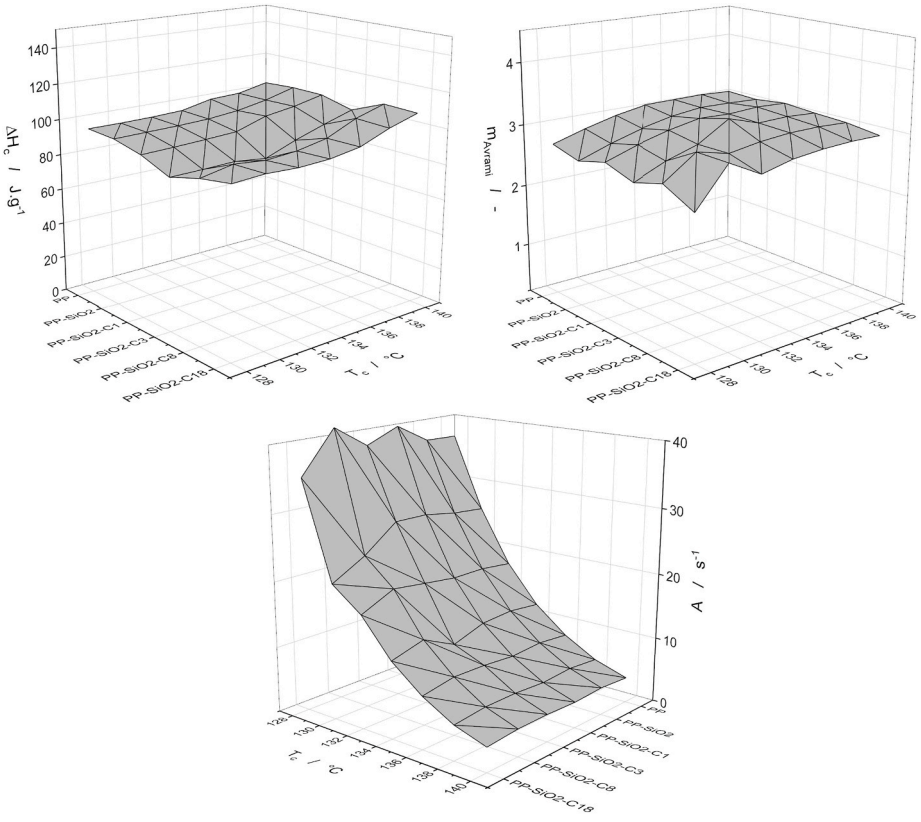

Fig. 11. Values of ΔH_c, m, and A determined by non-linear optimization for the isothermal crystallization data.

influence the crystallization rate of iPP, with shorter alkyl chains (C1) slowing it down, while longer chains (C3, C8, and C18) accelerate it. However, the changes occur primarily at the level of nucleation rather than crystal growth. Clear differences were demonstrated between organophilized and non-organophilized mixtures. The nature of the surface of organophilized SiO_2 particles changed from polar to non-polar, which had a positive effect on mixing and ultimately influenced the polymorphic composition and crystallization behavior of the studied mixtures.

CRediT authorship contribution statement

David Jaska: Writing – review & editing, Writing – original draft, Visualization, Validation, Methodology, Investigation, Formal analysis, Data curation, Conceptualization. **Jana Navratilova:** Writing – review & editing, Writing – original draft, Visualization, Validation, Supervision, Resources. **Roman Svoboda:** Software, Formal analysis. **Sona Zenzingerova:** Formal analysis, Data curation. **Lenka Gajzlerova:** Writing – review & editing, Visualization, Resources. **Martina Polaskova:** Writing – review & editing, Visualization, Resources. **Roman Cermak:** Supervision, Methodology, Conceptualization.

Declaration of competing interest

The authors declare that they have no known competing financial interests or personal relationships that could have appeared to influence the work reported in this paper.

Appendix A. Supplementary data

Supplementary data to this article can be found online at https://doi.org/10.1016/j.polymertesting.2026.109085.

Data availability

Data will be made available on request.

References

[1] V. Siracusa, I. Blanco, Bio-Polyethylene (Bio-PE), Bio-Polypropylene (Bio-PP) and Bio-Poly(ethylene terephthalate) (Bio-PET): recent developments in Bio-Based polymers analogous to petroleum-derived ones for packaging and engineering applications, Polymers 12 (2020) 1641, https://doi.org/10.3390/polym12081641.

[2] M. Amjadi, A. Fatemi, Tensile behavior of high-density polyethylene including the effects of processing technique, thickness, temperature, and strain rate, Polymers 12 (2020) 1857, https://doi.org/10.3390/polym12091857.

[3] L. Gajzlerova, J. Navratilova, S. Zenzingerova, D. Jaska, L. Benicek, M. Kudlacek, et al., On isotactic polypropylene annealing: difference in final properties of neat and β-nucleated polypropylene, Express Polym. Lett. 16 (2022) 453–464, https://doi.org/10.3144/expresspolymlett.2022.34.

[4] J. Kotek, I. Kelnar, J. Baldrian, M. Raab, Structural transformations of isotactic polypropylene induced by heating and UV light, Eur. Polym. J. 40 (2004) 2731–2738, https://doi.org/10.1016/j.eurpolymj.2004.07.017.

[5] S. Bruckner, S.V. Meille, Polymorphism in Crystalline Polypropylene, 1999, pp. 606–614, https://doi.org/10.1007/978-94-011-4421-6_82.

[6] J. Varga, Supermolecular structure of isotactic polypropylene, J. Mater. Sci. 27 (1992) 2557–2579, https://doi.org/10.1007/BF00540671.

[7] L. Chvatalova, J. Navratilova, R. Cermak, M. Raab, M. Obadal, Joint effects of molecular structure and processing history on specific nucleation of isotactic polypropylene, Macromolecules 42 (2009) 7413–7417, https://doi.org/10.1021/ma9005878.

[8] J. Vychopnova, R. Cermak, M. Obadal, V. Verney, S. Commereuc, Effect of β-nucleation on crystallization of photodegraded polypropylene, J. Therm. Anal. Calorim. 95 (2009) 215–220, https://doi.org/10.1007/s10973-008-8892-7.

[9] C. Grein, Toughness of neat, rubber modified and filled β-nucleated polypropylene: from fundamentals to applications, 43–104, https://doi.org/10.1007/b136972, 2005.

[10] J. Varga, β-MODIFICATION of isotactic polypropylene: preparation, structure, processing, properties, and application, J. Macromol. Sci. B 41 (2002) 1121–1171, https://doi.org/10.1081/MB-120013089.

[11] W. Qin, Z. Xin, C. Pan, S. Sun, X. Jiang, S. Zhao, In situ formation of zinc phthalate as a highly dispersed β-nucleating agent for mechanically strengthened isotactic polypropylene, Chem. Eng. J. 358 (2019) 1243–1252, https://doi.org/10.1016/j.cej.2018.10.108.

[12] X. Zhang, W. Qin, T. Wu, S. Zhao, A new insight into the formation of β-crystals of isotactic polypropylene induced by zinc dicarboxylic acids, Polymer (Guildf.) 262 (2022) 125500, https://doi.org/10.1016/j.polymer.2022.125500.

[13] Y. Yue, D. Hu, Q. Zhang, J. Lin, J. Feng, The effect of structure evolution upon heat treatment on the beta-nucleating ability of calcium pimelate in isotactic polypropylene, Polymer (Guildf.) 149 (2018) 55–64, https://doi.org/10.1016/j.polymer.2018.06.060.

[14] R. Cermak, M. Obadal, P. Ponizil, M. Polaskova, K. Stoklasa, A. Lengalova, Injection-moulded α- and β-polypropylenes: I. Structure vs. processing parameters, Eur. Polym. J. 41 (2005) 1838–1845, https://doi.org/10.1016/j.eurpolymj.2005.02.020.

[15] D. Libster, A. Aserin, N. Garti, Advanced nucleating agents for polypropylene, Polym. Adv. Technol. 18 (2007) 685–695, https://doi.org/10.1002/pat.970.

[16] M. Tolinski, Overview of fillers and fiber. Additives for Polyolefins - Getting the Most out of Polypropylene, Polyethylene and TPO, second ed., Elsevier, 2015.

[17] J. Murphy, Modifying specific properties: mechanical properties — filler. Additives for Plastics Handbook, Elsevier, 2001.

[18] T. Kuila Ttjhl, Polyolefin-based polymer nanocompositesfin-based polymer nanocomposite. Advances in Polymer Nanocomposites - Types and Applications, Woodhead Publishing, 2012.

[19] S. Nagasawa, A. Fujimori, T. Masuko, M. Iguchi, Crystallisation of polypropylene c ontaining nucleators, Polymer (Guildf.) 46 (2005) 5241–5250, https://doi.org/10.1016/j.polymer.2005.03.099.

[20] N. Ning, S. Fu, W. Zhang, F. Chen, K. Wang, H. Deng, et al., Realizing the enhancement of interfacial interaction in semicrystalline polymer/filler composites via interfacial crystallization, Prog. Polym. Sci. 37 (2012) 1425–1455, https://doi.org/10.1016/j.progpolymsci.2011.12.005.

[21] A.K. Schlarb, D.N. Suwitaningsih, M. Kopnarski, G. Niedner-Schatteburg, Supermolecular morphology of polypropylene filled with nanosized silica, J. Appl. Polym. Sci. 131 (2014), https://doi.org/10.1002/app.39655 n/a-n/a.

[22] A. Pustak, I. Pucic, M. Denac, I. Svab, J. Pohleven, V. Musil, et al., Morphology of polypropylene/silica nano- and microcomposites, J. Appl. Polym. Sci. 128 (2013) 3099–3106, https://doi.org/10.1002/app.38487.

[23] C. Tsioptsias, K. Leontiadis, E. Tzimpilis, I. Tsivintzelis, Polypropylene nanocomposite fibers: a review of current trends and new developments, J. Plast. Film Sheeting 37 (2021) 283–311, https://doi.org/10.1177/8756087920972146.

[24] M. Janicek, M. Polaskova, R. Holubar, R. Cermak, Surface-esterified cellulose fiber in a polypropylene matrix: impact of esterification on crystallization kinetics and dispersion, Cellulose 21 (2014) 4039–4048, https://doi.org/10.1007/s10570-014-0404-2.

[25] D.N. Bikiaris, A. Vassiliou, E. Pavlidou, G.P. Karayannidis, Compatibilisation effect of PP-g-MA copolymer on iPP/SiO2 nanocomposites prepared by melt mixing, Eur. Polym. J. 41 (2005) 1965–1978, https://doi.org/10.1016/j.eurpolymj.2005.03.008.

[26] F. Berzin, J.-J. Flat, B. Vergnes, Grafting of maleic anhydride on polypropylene by reactive extrusion: effect of maleic anhydride and peroxide concentrations on reaction yield and products characteristics, J. Polym. Eng. 33 (2013) 673–682, https://doi.org/10.1515/polyeng-2013-0130.

[27] L.A. Castillo, S.E. Barbosa, N.J. Capiati, Influence of talc morphology on the mechanical properties of talc filled polypropylene, J. Polym. Res. 20 (2013) 152, https://doi.org/10.1007/s10965-013-0152-2.

[28] B. Pukanszky, J. Moczo, Morphology and properties of particulate filled polymers, Macromol. Symp. 214 (2004) 115–134, https://doi.org/10.1002/masy.200451009.

[29] L.A. Castillo, S.E. Barbosa, Comparative analysis of crystallization behavior induced by different mineral fillers in polypropylene nanocomposites, Nanomater. Nanotechnol. 10 (2020) 184798042092275, https://doi.org/10.1177/1847980420922752.

[30] M. Naiki, Y. Fukui, T. Matsumura, T. Nomura, M. Matsuda, The effect of talc on the crystallization of isotactic polypropylene, J. Appl. Polym. Sci. 79 (2001) 1693–1703, https://doi.org/10.1002/1097-4628(20010228)79:9<1693::AID-APP190>3.0.CO;2-P.

[31] L.A. Castillo, S.E. Barbosa, N.J. Capiati, Influence of talc genesis and particle surface on the crystallization kinetics of polypropylene/talc composites, J. Appl. Polym. Sci. 126 (2012) 1763–1772, https://doi.org/10.1002/app.36846.

[32] Z. Ren, R.A. Shanks, T.J. Rook, Crystallization and melting of highly filled polypropylene composites prepared with surface-treated fillers, J. Appl. Polym. Sci. 79 (2001) 1942–1948, https://doi.org/10.1002/1097-4628(20010314)79:11<1942::AID-APP1001>3.0.CO;2-P.

[33] F. Rybnikar, Interactions in the system isotactic polypropylene–calcite, J. Appl. Polym. Sci. 42 (1991) 2727–2737, https://doi.org/10.1002/app.1991.070421011.

[34] T. Kowalewski, A. Galeski, Influence of chalk and its surface treatment on crystallization of filled polypropylene, J. Appl. Polym. Sci. 32 (1986) 2919–2934, https://doi.org/10.1002/app.1986.070320107.

[35] T. Labour, C. Gauthier, R. Seguela, G. Vigier, Y. Bomal, G. Orange, Influence of the β crystalline phase on the mechanical properties of unfilled and CaCO 3 -filled polypropylene. I. Structural and mechanical characterisation, Polymer (Guildf.) 42 (2001) 7127–7135, https://doi.org/10.1016/S0032-3861(01)00089-1.

[36] M. Avella, S. Cosco, M.L. Di Lorenzo, E. Di Pace, M.E. Errico, G. Gentile, Nucleation activity of nanosized CaCO3 on crystallization of isotactic polypropylene, in dependence on crystal modification, particle shape, and coating, Eur. Polym. J. 42 (2006) 1548–1557, https://doi.org/10.1016/j.eurpolymj.2006.01.009.

[37] H. Tang, Q. Dong, P. Liu, Y. Ding, F. Wang, C. Gao, et al., Isothermal crystallization of polypropylene/surface modified silica nanocomposites, Sci. China: Chem. 59 (2016) 1283–1290, https://doi.org/10.1007/s11426-016-0146-0.

[38] S.L. Blagojevic, Z. Buhin, I. Igrec, Influence of silica nanofiller on the isothermal crystallization and melting of polyurethane elastomer, J. Appl. Polym. Sci. 129 (2013) 1466–1475, https://doi.org/10.1002/app.38846.
[39] G.Z. Papageorgiou, D.S. Achilias, D.N. Bikiaris, G.P. Karayannidis, Crystallization kinetics and nucleation activity of filler in polypropylene/surface-treated SiO2 nanocomposites, Thermochim. Acta 427 (2005) 117–128, https://doi.org/10.1016/j.tca.2004.09.001.
[40] H. Tang, Q. Dong, P. Liu, Y. Ding, F. Wang, C. Gao, et al., Isothermal crystallization of polypropylene/surface modified silica nanocomposites, Sci. China: Chem. 59 (2016) 1283–1290, https://doi.org/10.1007/s11426-016-0146-0.
[41] S. Song, X. Wang, R. Mu, Z. Xing, D. Xiying, Performance evaluation of polypropylene resin for capacitor film, J Phys Conf Ser 2009 (2021) 012003, https://doi.org/10.1088/1742-6596/2009/1/012003.
[42] D. Kregiel, Advances in biofilm control for food and beverage industry using organo-silane technology: a review, Food Control 40 (2014) 32–40, https://doi.org/10.1016/J.FOODCONT.2013.11.014.
[43] W. Stober, A. Fink, E. Bohn, Controlled growth of monodisperse silica spheres in the micron size range, J. Colloid Interface Sci. 26 (1968) 62–69, https://doi.org/10.1016/0021-9797(68)90272-5.
[44] P.A. Bazuła, P.M. Arnal, C. Galeano, B. Zibrowius, W. Schmidt, F. Schuth, Highly microporous monodisperse silica spheres synthesized by the Stober process, Microporous Mesoporous Mater. 200 (2014) 317–325, https://doi.org/10.1016/j.micromeso.2014.07.051.
[45] E.G. Barrera, P.R. Livotto, J.H.Z. dos Santos, Hybrid silica bearing different organosilanes produced by the modified Stober method, Powder Technol. 301 (2016) 486–492, https://doi.org/10.1016/j.powtec.2016.04.025.
[46] G. Chen, S. Zhou, G. Gu, L. Wu, Modification of colloidal silica on the mechanical properties of acrylic based polyurethane/silica composites, Colloids Surf. A Physicochem. Eng. Asp. 296 (2007) 29–36, https://doi.org/10.1016/j.colsurfa.2006.09.016.
[47] H. Chen, S. Zhou, G. Gu, L. Wu, Study on modification and dispersion of Nano-silica, J. Dispersion Sci. Technol. 26 (2005) 27–37, https://doi.org/10.1081/DIS-200040232.
[48] E. Moretto, J.P.C. Fernandes, M. Staropoli, V. Roge, P. Steiner, B. Duez, et al., Dual-Silane premodified Silica nanoparticles—synthesis and interplay between Chemical, mechanical, and curing properties of Silica–Rubber nanocomposites: application to tire tread compounds, ACS Omega 7 (2022) 17692–17702, https://doi.org/10.1021/acsomega.2c00665.
[49] X. Zhang, D. Zhang, T. Liu, Influence of nucleating agent on properties of isotactic polypropylene, Energy Proc. 17 (2012) 1829–1835, https://doi.org/10.1016/J.EGYPRO.2012.02.319.
[50] F. Lin, M. Zhang, T. Zhao, Y. Zhang, D. Ning, W. Cui, et al., Exploitation of a new nucleating agent by molecular structure modification of Aryl Phosphate and its effect on application properties of the polypropylene, Polymers 15 (2023) 4730, https://doi.org/10.3390/POLYM15244730.
[51] L. Cui, P. Wang, Y. Zhang, L. Zhang, Y. Chen, L. Wang, et al., Combined effect of α-nucleating agents and glass fiber reinforcement on a polypropylene composite: a balanced approach, RSC Adv. 7 (2017) 42783–42791, https://doi.org/10.1039/C7RA08322J.
[52] L. Gajzlerova, J. Navratilova, S. Zenzingerova, D. Jaska, L. Benicek, M. Kudlacek, et al., On isotactic polypropylene annealing: difference in final properties of neat and β-nucleated polypropylene, Express Polym. Lett. 16 (2022) 453–464, https://doi.org/10.3144/expresspolymlett.2022.34.
[53] A. Turner-Jones, A.J. Cobbold, The β crystalline form of isotactic polypropylene, J. Polym. Sci. B 6 (1968) 539–546, https://doi.org/10.1002/POL.1968.110060802.
[54] A.T. Jones, J.M. Aizlewood, D.R. Beckett, Crystalline forms of isotactic polypropylene, Makromol. Chem. 75 (1964) 134–158, https://doi.org/10.1002/MACP.1964.020750113.
[55] F.J. Lanyi, N. Wenzke, J. Kaschta, D.W. Schubert, On the determination of the enthalpy of fusion of α-Crystalline isotactic polypropylene using differential scanning calorimetry, X-Ray diffraction, and fourier-transform infrared spectroscopy: an old story revisited, Adv. Eng. Mater. 22 (2020), https://doi.org/10.1002/ADEM.201900796.
[56] J. Krajenta, A. Pawlak, Crystallization of the β-Form of polypropylene from the melt with reduced entanglement of macromolecules, Polymers 16 (2024) 1710, https://doi.org/10.3390/POLYM16121710, 2024;16:1710.
[57] D. Li, Y. Xin, Y. Song, T. Dong, H. Ben, R. Yu, et al., Crystalline modification of isotactic polypropylene with a rare Earth nucleating agent based on ultrasonic vibration, Polymers 11 (2019) 1777, https://doi.org/10.3390/POLYM11111777, 2019;11:1777.
[58] H. Yoshida, Dynamic analysis of the melting behavior of polymers showing polymorphism observed by simultaneous DSC/X-ray diffraction measurements, Thermochim. Acta 267 (1995) 239–248, https://doi.org/10.1016/0040-6031(95)02482-4.
[59] F.J. Padden, H.D. Keith, Spherulitic crystallization in polypropylene, J. Appl. Phys. 30 (1959) 1479–1484, https://doi.org/10.1063/1.1734985.
[60] A. Menyhard, J. Varga, G. Molnar, Comparison of different -nucleators for isotactic polypropylene, characterisation by DSC and temperature-modulated DSC (TMDSC) measurements, J. Therm. Anal. Calorim. 83 (2006) 625–630, https://doi.org/10.1007/s10973-005-7498-6.
[61] Y. Guan, S. Wang, A. Zheng, H. Xiao, Crystallization behaviors of polypropylene and functional polypropylene, J. Appl. Polym. Sci. 88 (2003) 872–877, https://doi.org/10.1002/app.11668.
[62] G. Zhang, J. Yu, Z. Xin, Q. Gui, S. Wang, Crystallization kinetics of nucleated polypropylene with organic phosphates, J. Macromol. Sci. B 42 (2003) 663–675, https://doi.org/10.1081/MB-120021597.
[63] J. Varga, K. Stoll, A. Menyhard, Z. Horvath, Crystallization of isotactic polypropylene in the presence of a β-nucleating agent based on a trisamide of trimesic acid, J. Appl. Polym. Sci. 121 (2011) 1469–1480, https://doi.org/10.1002/app.33685.
[64] H. Bai, Y. Wang, Q. Zhang, L. Liu, Z. Zhou, A comparative study of polypropylene nucleated by individual and compounding nucleating agents. I. Melting and isothermal crystallization, J. Appl. Polym. Sci. 111 (2009) 1624–1637, https://doi.org/10.1002/app.29153.
[65] Z. Wei, W. Zhang, G. Chen, J. Liang, S. Yang, P. Wang, et al., Crystallization and melting behavior of isotactic polypropylene nucleated with individual and compound nucleating agents, J. Therm. Anal. Calorim. 102 (2010) 775–783, https://doi.org/10.1007/s10973-010-0725-9.
[66] J. Kang, J. Zhang, Z. Chen, F. Yang, J. Chen, Y. Cao, et al., Isothermal crystallization behavior of β-nucleated isotactic polypropylene with different melt structures, J. Polym. Res. 21 (2014) 506, https://doi.org/10.1007/s10965-014-0506-4.
[67] J. Varga, Melting and Supermolecular Structure of Isotactic Polypropylene, 1, Chapman & Hall, London, 1995. Crystallization.
[68] J. Sestak, Thermophysical Properties of Solids - Their Measurements and Theoretical Thermal Analysis , aus der Reihe: comprehensive Analytical Chemistry, in: G. Svehla (Ed.), Subseries of Monographs on Thermal Analysis, 89, 1985, https://doi.org/10.1002/bbpc.19850890630. W. W. Wendlandt: Vol. XII, Part D. Elsevier Science Publishers, Amsterdam and New York 1984. 440 Seiten, 122 Abbildungen, Ganzleinen US $ 115,50/Dfl. 300,-. Berichte Der Bunsengesellschaft Für Physikalische Chemie:721–721.
[69] J.D. Hoffman Gtdjiljr, Treatise on solid State chemistry, New Yok: N. B. Hannay 3 (1976).
[70] M. Avrami, Granulation, phase change, and microstructure – kinetics of phase change III, J. Chem. Phys. 7 (1941).
[71] M. Avrami, Kinetics of phase change. II–transformation-time relations for random distribution of nuclei, J. Chem. Phys. 7 (1940).
[72] W.A. Johnson Kfm, Reaction kinetics in processes of nucleation and growth, Trans. Am. Inst. Min. (Metall) Eng. 135 (1939).
[73] M. Avrami, Kinetics of phase change I–general theory, J. Chem. Phys. 7 (1939).
[74] R. Svoboda, Crystallization of glasses – when to use the johnson-mehl-avrami kinetics? J. Eur. Ceram. Soc. 41 (2021) 7862–7867, https://doi.org/10.1016/j.jeurceramsoc.2021.08.026.
[75] F. Deckers, K. Rasim, C. Schröder, Molecular dynamics simulation of polypropylene: diffusion and sorption of H2O, H2O2, H2, O2 and determination of the glass transition temperature, J. Polym. Res. 29 (2022) 463, https://doi.org/10.1007/s10965-022-03304-y.
[76] H. Asakawa, K. Nishida, T. Kanaya, M. Tosaka, Giant single crystal of isotactic polypropylene showing near-equilibrium melting temperature, Polym. J. 45 (2013) 287–292, https://doi.org/10.1038/pj.2012.136.
[77] T. Huang, C. Zhou, Surface diffusion-controlled jonhson–mehl–avrami–kolmogorov model for hydrogenation of Mg-based alloys, J. Phys. Chem. C 127 (2023) 13900–13910, https://doi.org/10.1021/acs.jpcc.3c02650.